Observation of charge transfer in mixed-dimensional heterostructures formed by transition metal dichalcogenide monolayers and PbS quantum dots

Peymon Zereshki,[1] Mohammad Mahdi Tavakoli,[2] Pavel Valencia-Acuna,[1] Ji-Hoon Park,[2] Jing Kong,[2] and Hui Zhao[1,*]

[1]*Department of Physics and Astronomy, The University of Kansas, Lawrence, Kansas 66045, United States*

[2]*Department of Electrical Engineering and Computer Science, Massachusetts Institute of Technology, Cambridge, Massachusetts 02139, United States*

(Dated: November 8, 2019)

Abstract

We report an experimental study on charge transfer properties of mixed-dimensional heterostructures formed by zero-dimensional PbS quantum-dots and two-dimensional transition metal dichalcogenides. Monolayers of $MoSe_2$ and MoS_2 were fabricated by mechanical exfoliation and chemical vapor deposition techniques, respectively. PbS quantum dots with diameters of 2.3 nm and 5 nm were synthesized by a hot-injection method and characterized by optical absorption spectroscopy and ultraviolet photoemission spectroscopy. The quantum dots were deposited on the MoS_2 and $MoSe_2$ monolayers to form heterostructures. Photoluminescence and transient absorption measurements were performed on the heterostructures as well as individual materials to reveal their photocarrier dynamics. We found that the holes excited in $MoSe_2$ can efficiently transfer to both 2.3-nm and 5-nm PbS quantum dots, while electrons in these quantum dots cannot transfer to $MoSe_2$. Similar charge transfer properties were observed between MoS_2 and the 5-nm PbS quantum dots, while no charge transfer was observed between MoS_2 and the 2.3-nm quantum dots. These results provide useful information for understanding the physical mechanism of charge transfer in mixed-dimensional heterostructures and for developing PbS quantum-dot-based mixed-dimensional materials.

I. INTRODUCTION

The discovery of graphene[1] has created rapidly growing interests in two-dimensional (2D) materials, such as transition metal dichalcogenides (TMDs)[2]. These atomically thin materials possess several unique features that are attractive to fundamental research and applications. One intriguing aspect of 2D materials is that they provide a new route to fabricating heterostructures[3]. Initial efforts on this research direction have been focused on vertical heterostructures formed by two 2D materials *via* van der Waals interactions[4,5]. In just a few years, significant progress has been made on fabricating such heterostructures, understanding their properties, and exploring their potential applications. However, one limit of the 2D-2D heterostructures is that, for a certain material combination, the electronic bands and their alignment are fixed. To gain more tunability of the electronic and optical properties, one natural thought was to utilize an additional dimension by introducing quantum confinement in the lateral direction. In this regard, quantum dots (QDs) offer great flexibility on tuning their electronic structures by the size. Thus, combining QDs with 2D materials in the so-called 0D-2D heterostructures can open up new methods to engineer and control the band alignment and charge transfer properties, which are key elements to harnessing emergent optoelectronic properties in these heterostructures.

Recent efforts on developing 0D-2D heterostructures have focused on CdSe-based core-shell QDs, which have been known as a model 0D system since early 2000[6,7]. In such QDs, the bandgap of CdSe can be controlled by their size, utilizing the quantum confinement effect. This allows control of their photon absorption and emission energies. Furthermore, by choosing different shell materials, both type-I[6] and type-II band alignments of the core-shell structure[7] can be achieved, enabling fine control of the spatial distribution of the electrons and holes. Very recently, efficient electron transfer, including charge transfer and energy transfer, has been observed in the heterostructures formed by CdSe QDs and several 2D TMDs, including MoS_2[8–12], $MoSe_2$[13], and SnS_2[14], providing an important mechanism to combine novel properties of the individual materials for electronic and optoelectronic applications. Indeed, 0D-2D heterostructures involving CdSe as well as other QDs have been used to fabricate phototransistors[15–19], photovoltaics[20], and memory devices[21,22]. However, several key aspects of electron transfer in CdSe-based 0D-2D heterostructures are still under debate, such as the effect of the thickness of the 2D layer[10,12,14], the mechanisms of the electric-field-dependent energy transfer[9], modeling the energy transfer mechanisms to account for the distance dependence of the transfer rate[9,10,13], and the efficiency of charge

transfer across the shell barriers[23].

To expand the material library for 0D-2D heterostructures and to provide more insight for understanding electron transfer mechanisms in such heterostructures, we studied charge transfer between PbS QDs and TMDs, including $MoSe_2$ and MoS_2. PbS QDs are one of the most commonly used nanomaterials as light absorbers[24,25]. Their narrow and tunable bandgaps covering a spectral range from 0.4 to 1.5 eV make them an ideal choice for optoelectronic devices in the near infrared region[25]. Recently, PbS QDs have been successfully applied in infrared light emitting diodes, infrared and near infrared photodetectors, multijunction solar cells, and telecommunication devices[25–27]. From a fundamental point of view, without a shell layer, PbS QDs could offer a simpler model system to study the physical mechanism of charge transfer between 0D and 2D systems.

Using PbS QDs with different diameters, we studied the charge transfer process in TMDs/PbS QDs heterostructures by using transient absorption and steady-state photoluminescence (PL) spectroscopy. We found that holes injected in monolayer $MoSe_2$ can transfer to both 5-nm and 2.3-nm PbS QDs, which is consistent with the type-II band alignment of such heterostructures. However, electron transfer from QDs to $MoSe_2$ is insignificant. Similar charge transfer properties were observed in the heterostructure formed by monolayer MoS_2 and 5-nm PbS QDs. However, charge transfer is absent between MoS_2 and 2.3-nm QDs. These results provide useful information for understanding mechanisms of charge transfer in 0D-2D heterostructure and for developing PbS QD-based mixed-dimensional materials.

II. EXPERIMENTAL METHODS

A. Sample Fabrication

$MoSe_2$ monolayers were mechanically exfoliated from bulk crystals on polydimethylsiloxane substrates with a thickness of about 1 mm. The linear proportionality between the thickness and the green-channel contrast[28–30] was used to identify the monolayer flakes, which were transferred to the Si/SiO_2 substrates. MoS_2 monolayers were synthesized by metal-organic chemical vapor deposition on Si/SiO_2 substrates under low pressures. The precursors for Mo and S were molybdenum hexacarbonyl (98 %, Sigma Aldrich) and diethyl sulfide (98 %, Sigma Aldrich), respectively. These precursors were supplied in a gaseous phase by a bubbler system. During the growth, the

flow rates for argon, molybdenum hexacarbonyl and diethyl sulfide were 100, 0.6, and 2.0 sccm, respectively. The growth was at a substrate temperature of 400°C and lasted for 15 hours.

PbS QDs were synthesized using a hot injection method, as reported elsewhere[31–34]. Briefly, 7 g of oleic acid and 10 mmol of lead acetate trihydrate were mixed in a three-neck flask and dissolved in 60 g of 1-octadecene with vigorous stirring. Then, the mixture was heated up to 100°C under vacuum overnight to prepare the lead precursor. For sulfide precursor, 1 mL of hexamethyldisilathiane and 9 mL of 1-octadecene were mixed. The PbS QDs was formed by rapid injection of the sulfide precursor into the lead precursor solution. The QDs with diameters of 2.3 and 5 nm were obtained by setting the temperature at 75°C for 10 min and 180°C for 2 min, respectively. After quenching, the QDs were purified using a mixture of hexane and isopropanol. Finally, the QDs were redistributed in octane with concentrations of 10 mg mL^{-1} for 2.3-nm QDs and 5 mg/mL for 5-nm QDs.

In order to deposit the PbS QDs on TMD monolayers, 40 μL of the solution was deposited on TMD monolayers using spin coating at 2500 rpm for 30 s. For ligand exchange purposes, a solution of 1,2-Ethanedithiol diluted concentration 0.02 % vol in acetonitrile was dropped on top of the PbS QDs film. The QDs were exposed to the 1,2-Ethanedithiol for 25 s, before spin drying, followed by 3 times rinsing with acetonitrile. The thickness of the QDs layer was about 5 nm, measured by Alpha-Step 200 (Tencor). For each heterostructure, two samples were fabricated and studied, and similar results were obtained.

B. Optical Measurements

Photoluminescence spectroscopic measurements were performed with a homemade setup. A 405-nm continuous-wave laser was used as the excitation source. The laser beam was focused on the sample with a spot size of about 2 μm by an objective lens. The PL was collected in the reflection geometry and detected by a Horiba HR550 spectrometer equipped with a thermoelectrically cooled charge-coupled-device camera. UV-visible measurement was performed by a Varian Cary 5000 UV-VIS-NIR absorption spectrometer.

Charge transfer and the dynamics of photocarriers in the samples fabricated were studied by a homemade femtosecond pump-probe setup. An 80-MHz passive mode-locked Ti:sapphire laser generates 100 fs pulses with a central wavelength of about 780 - 790 nm. A portion of this output is sent to a nonlinear optical crystal to generate its second harmonic pulses of about 390 - 395

nm. The rest of the output is used to pump an optical parametric oscillator, which produces near-infrared pulses. The second harmonic of these pulses in the range of 610 - 670 nm are generated in another nonlinear optical crystal. Depends on the experimental configurations, two of these pulses are selected as the pump and probe, which are combined by a beamsplitter and co-focused on the sample by a microscope objective lens. The reflection of the probe beam was sent to a photodiode. The unwanted pump reflection was blocked by using appropriate filters in front of the photodiode. The output of the photodiode is measured by a lock-in amplifier, with the pump beam being modulated at a frequency of about 2 KHz by a mechanical chopper. The differential reflection of the probe is measured as a function of the probe delay (defined as the arrival time of the probe pulse at the sample with respect to the pump pulse) by changing the probe path length. The differential reflection is defined as $\Delta R/R_0 = (R - R_0)/R_0$, where R and R_0 are the probe reflectance with and without the presence of the pump, respectively. This quantity monitors the density of photocarriers injected by the pump pulse[35]. All the measurements were performed with the sample in ambient condition at room temperature.

III. RESULTS AND DISCUSSION

A. PbS Quantum Dots

Figure 1 shows basic characterization of the PbS QDs. We measured the ultraviolet photoelectron spectra of the 5-nm QDs, as shown in Figure 1(a) and (b). We extracted a Fermi level of -4.18 eV and the highest occupied molecular orbital (HOMO) of -4.50 eV (both with respect to the vacuum level). Figure 1(c) and (d) show the similar measurement of the 2.3-nm QDs, which yields the Fermi level and the HOMO of -4.42 and -5.10 eV, respectively. As seen in Figure 1(e), the 5-nm QDs show an absorption peak at about 1390 nm. The energy gap of 0.89 eV confirms their diameter, based on previously reported results[25]. Using this value, we deduce its lowest unoccupied molecular orbital (LUMO) of -3.61 eV, as shown in the inset. Panel (f) shows the absorption spectrum and the energy diagram of the 2.3-nm QDs deduced with the same method. Based on these results, both QDs are p-type doped.

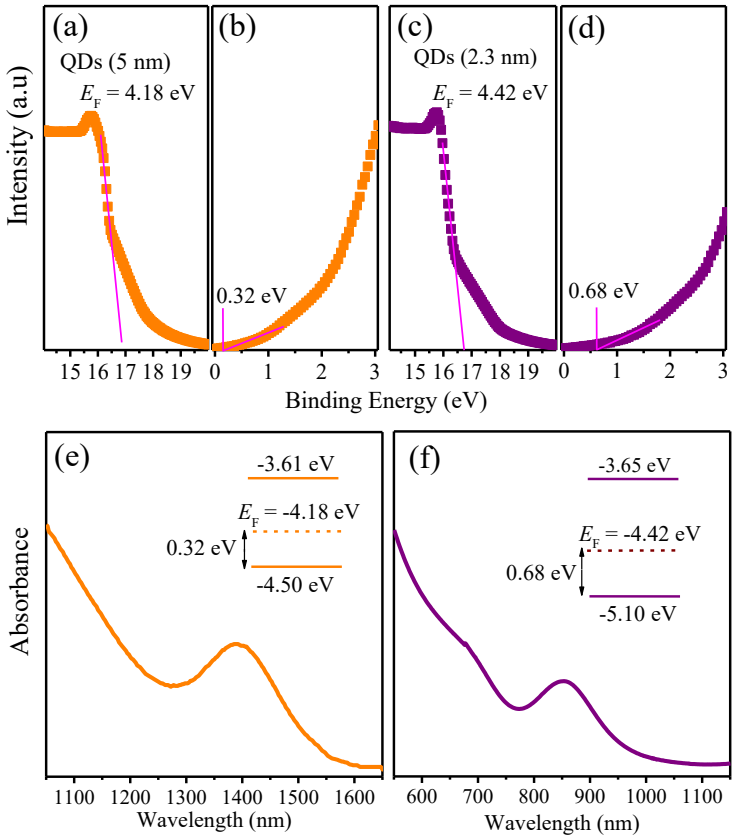

FIG. 1. (a) and (b): Ultraviolet photoelectron spectra of the 5-nm PbS QDs. (c) and (d): Same as (a) and (b) but for 2.3-nm QDs. In both cases, the thickness of the QD films is 5 nm. (e) and (f): Absorbance of the films of QDs diameters of 5 and 2.3 nm, respectively. The insets show the lowest unoccupied molecular orbitals (upper lines), the highest occupied molecular orbitals (lower lines), and the Fermi levels (dashed lines), all with respect to the vacuum level.

B. Charge Transfer between $MoSe_2$ Monolayer and PbS Quantum Dots

Figure 2(a) shows an optical microscope image of a $MoSe_2$ monolayer fabricated by mechanical exfoliation. After the exfoliation, a 5-nm film of the PbS QDs with a diameter of 5 nm was deposited, as shown in (b). Figure 2(c) illustrates the expected band alignment of the $MoSe_2$/PbS QDs (5 nm) heterostructure, according to the energy diagram of the QDs obtained in Figure 1 and the previous reported electronic structures of monolayer $MoSe_2$[36]. The LUMO of the QDs (-3.61 eV) is 250 meV higher than the bottom of the conduction band of $MoSe_2$ (-3.86 eV), while the HOMO of the QDs (-4.50 eV) is 890 meV higher than the top of the valence band of $MoSe_2$ (-5.41). Hence, the $MoSe_2$ and the 5-nm QDs are expected to form a type-II band alignment,

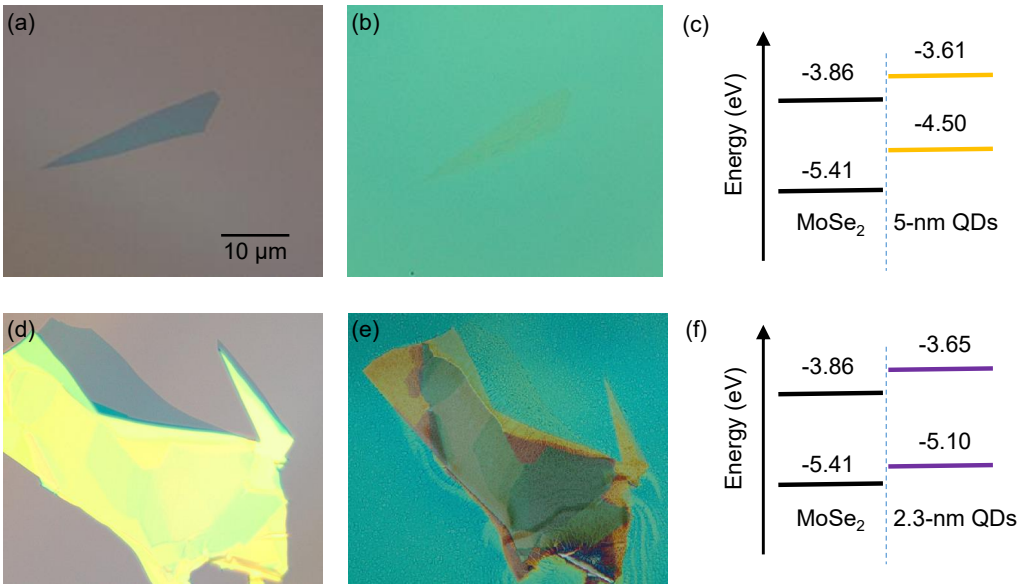

FIG. 2. (a) Optical microscope image of a $MoSe_2$ monolayer on a Si/SiO_2 substrate. (b) The same monolayer after after deposition of a 5-nm film of PbS QDs with a diameter of 5 nm. (c) The band alignment of the $MoSe_2$/QDs (5 nm) heterostructure shown in (b). The energy levels of the PbS QDs are measured by ultraviolet photoelectron spectroscopy (see the text). The energy bands of $MoSe_2$ are adopted from theory[36]. (d - f) Same as (a - c) but with QD diameters of 2.3 nm.

which allows electron transfer from QDs to $MoSe_2$ and hole transfer along the opposite direction. Similar to Panels (a), (b), and (c) of Figure 2, Panels (d), (e), and (f) show the $MoSe_2$ monolayer, the heterostructure, and the expected band alignment, respectively, with the 2.3-nm-diameter QDs. The band alignment is also type-II, but with smaller valence band offset than the heterostructure based on the 5-nm QDs.

We first performed PL spectroscopy to probe the potential charge transfer process. Figure 3 shows the PL spectra obtained from several samples. A 405-nm continuous-wave laser beam with an incident power of 5 μW and a focused spot size of about 2 μm was used for excitation. The $MoSe_2$ monolayer shows a strong PL peak centered at 783 nm (black). The PL spectrum of the 2.3-nm QDs (purple) has a broad peak from 700 to 850 nm. Interestingly, the spectrum of the heterostructure formed by $MoSe_2$ monolayer and the 2.3-nm QDs (blue) is significantly different from a simple sum of the spectra of the two individual materials. Specifically, the PL band associated with the QDs is increased by about a factor of 3, while the peak from $MoSe_2$ is reduced by a factor of about 35. Such a significant PL quenching of $MoSe_2$ indicates that a large

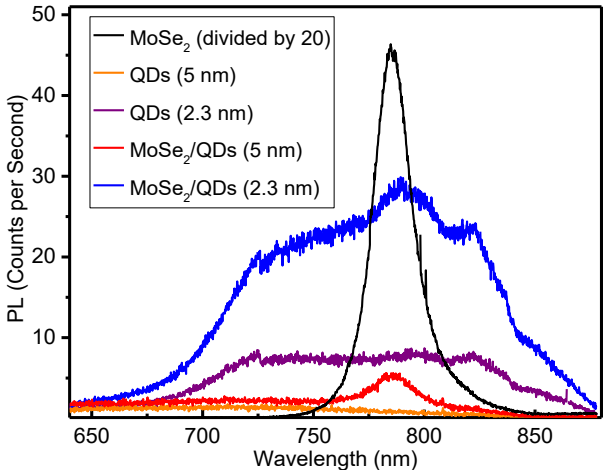

FIG. 3. Photoluminescence spectra of the $MoSe_2$ monolayer (black, divided by 20), the 5-nm PbS QDs (orange), the 2.3-nm PbS QDs (purple), the $MoSe_2$/QDs (5 nm) heterostructure (red), and the $MoSe_2$/QDs (2.3 nm) heterostructure (blue). All the spectra were measured under the same continuous-wave excitation of 405 nm and 5 μW.

portion of the photocarriers excited in $MoSe_2$ transfer to the QDs on a time scale much shorter than their recombination lifetime in $MoSe_2$[37,38]. This could be attributed to hole transfer from $MoSe_2$ to 2.3-nm QDs, as suggested by the type-II band alignment shown in Figure 2(f) or transfer of the electron-hole pairs (in form of energy transfer) from $MoSe_2$ to the QDs. The small increase of the QD PL could suggest a net gain of photocarriers by these QDs; however, we cannot rule out other factors such as the effect of the substrate on the PL yield. For the 5-nm QDs, no PL peak was detected in the spectral range of this study (orange), which is reasonable since their PL peak is expected to be at about 1400 nm. For the heterostructure formed by $MoSe_2$ and the 5-nm QDs, the peak from $MoSe_2$ is quenched by about 180 times (red), suggesting even more efficient transfer of photocarriers from $MoSe_2$ to the 5-nm QDs.

Next, we performed transient absorption measurements to time resolve the photocarrier transfer dynamics in these samples. We first studied the photocarrier dynamics in the $MoSe_2$ monolayer. A 1.87-eV pump pulse with an energy fluence of 16 μJ cm^{-2} was used to excite the sample. Since the optical bandgap of $MoSe_2$ is about 1.59 eV, the pump pulse injects photocarriers by interband absorption. The dynamics of these carriers is monitored by measuring the differential reflection of a 1.59-eV probe pulse, which is tuned to the optical bandgap of $MoSe_2$. The result is shown as the black symbols in Figure 4. As can be seen in the left panel, the signal reaches a peak shortly after

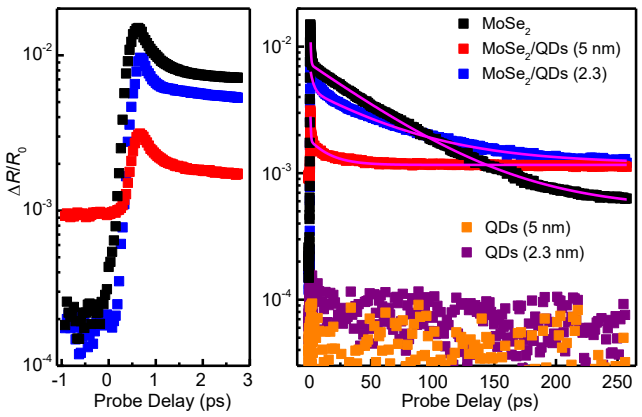

FIG. 4. Differential reflection signals with 1.87-eV pump and 1.58-eV probe measured from the $MoSe_2$ monolayer (black), 5-nm PbS QDs (orange), 2.3-nm PbS QDs (purple), the $MoSe_2$/QDs (5 nm) heterostructure (red), and the $MoSe_2$/QDs (2.3 nm) heterostructure (blue), all under the same conditions. The curves are exponential fits (see text).

the pump excitation, which shows that the injected photocarriers immediately produce a maximum differential reflection signal. The decay of the signal has three exponential components according to a fit, shown as the magenta curve over the data points. The time constants (and the weights) of the three components are $\tau_1 = 0.4 \pm 0.1$ ps (45%), $\tau_2 = 32 \pm 5$ ps (30%), and $\tau_3 = 90 \pm 11$ ps (25%). The sub-picosecond τ_1 process has been generally observed in TMD monolayers under interband excitations, and has been attributed to the exciton formation process from the injected free electron-hole pairs[39]. The 90-ps process could be attributed to the exciton lifetime[40], while the intermediate process of 32 ps could be due to the influence of additional processes on the excitonic dynamics, such as defect-assisted recombination or exciton-exciton annihilation. When the same measurement was performed on the 5-nm PbS QDs, no signal was detected, as shown by the orange symbols. This is reasonable since the probe photon energy is too far away from the resonant energy of about 0.9 eV to effectively detect photocarriers in the QDs.

We then studied the heterostructure sample formed by the $MoSe_2$ monolayer and the 5-nm PbS QDs under the same experimental conditions. Here, the pump excites both materials and the probe is expected to primarily sense photocarriers in $MoSe_2$. We observed a signal that is significantly different from $MoSe_2$, as shown by the red symbols in Figure 4. First, it has a large residual at negative delays, which is about 30 % of the the peak signal. Second, it has a long-lived signal at positive delays.

We attribute these features to the hole transfer process due to the type-II band alignment shown in Figure 2(c). First of all, if photocarrier transfer is absent, the signal from the heterostructure should show the same dynamics as the $MoSe_2$ monolayer since the carriers excited in QDs do not contributed to the signal. In contrast, the signal from the heterostructure show a decay process of about 15 ps after the initial sub-picosecond process (the magenta curve over the red symbols). We can thus attribute this 15-ps decay process of the signal to the transfer of holes from $MoSe_2$ to the PbS QDs, since after the transfer process the holes no longer contribute to the signal. The electrons excited in $MoSe_2$ are expected to reside in $MoSe_2$ since the energy level in the QDs are higher than $MoSe_2$ [Figure 2(c)]. They have extended lifetime due to the loss of the holes to the QDs as their recombination partners, resulting in the long-lived signal and the residual at negative delays (carrier buildup). This interpretation based on hole transfer and electron-hole separation is also consistent with the significant PL quenching observed in 3.

Our measurements were performed with an 80-MHz laser system, which has a pulse separation of about 13 ns. The significant residual observed at negative delays can be attributed to the partial recovery of the sample from each pulse excitation, due to the ultralong electron lifetime. Ideally, one would desire the measurements to be done with a pulse separation much larger than the lifetime so that the sample was fully recovered. Unfortunately, the pulse separation in our experimental setup is not tunable. However, this experimental issue does not impact our conclusion. The residual observed at negative delays reflects a steady-state population of photocarriers produced by all the pump pulses. Hence, the differential reflection observed at positive delays is the sum of this time-independent residual associated with the steady-state population and the actual signal produced by the photocarriers injected by one pump pulse (which decays with time, and which dynamics is measured). When analyzing the decay of the signal, the effect of the residual is removed by allowed a nonzero constant in the exponential fits.

To further confirm the origin of the long-lived signal and the residual, the measurement was repeated with various pump fluences. The results are summarized in Figure 5. Clearly, the dynamics is independent of the pump fluence and both the signal at positive delays and the residual at negative delays are proportional to the pump fluence, which is proportional to the injected carrier density. The small increase of the signal after 100 ps could be attributed to effects of lattice vibration or beam walkoff. However, this minor feature has no impact on the above conclusion.

Having established the hole transfer process from $MoSe_2$ to the 5-nm PbS QDs, which is consistent with the type-II band alignment shown in Figure 2(c), it is interesting to observe a potential

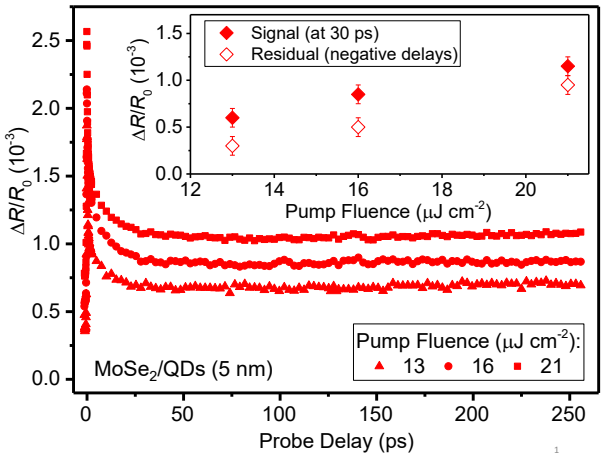

FIG. 5. Differential reflection signals from the $MoSe_2$/QDs (5 nm) heterostructure with different energy fluences of the pump pulse. The inset shows that both the signal (solid symbols) and the residual (open symbols) are proportional to the fluence.

electron transfer process from QDs to $MoSe_2$, which is allowed by this band alignment. This transfer process could be observed by detecting electrons in $MoSe_2$ of the heterostructure when only the QDs are excited. For this purpose, we first used a 1.59 eV pump pulse with an energy fluence of 22 μ J cm^{-2} to excite the heterostructure region. This pump injects photocarriers in both $MoSe_2$ and the QDs. We used a 1.86-eV probe to detect the B-exciton resonance of $MoSe_2$. The differential reflection signal observed are plotted in Figure 6 as the solid symbols. This measurement thus demonstrates that the 1.86-eV probe can effectively monitor carriers in $MoSe_2$. Next, we changed the pump photon energy to 1.52 eV, which is below the optical bandgap of $MoSe_2$ and thus can only excite the QDs. If the electrons excited in the QDs can transfer to $MoSe_2$, they can be detected by the probe. However, no signal was observed, as indicated by the open symbols in Figure 6. Therefore, we conclude that electrons in the 5-nm QDs do not transfer to $MoSe_2$, even though the band alignment allows so. We note that the band alignment is not a sufficient condition for charge transfer, as has been confirmed in other van der Waals heterostructures[41,42]. Here, we attribute the lack of electron transfer from QDs to $MoSe_2$ the localized nature of the electrons in the QDs, which limits their coupling with the states in $MoSe_2$, and the relatively smaller band offset of the conduction bands compared to the valence bands [Figure 2(c)].

The charge transfer property of the heterostructure formed by monolayer $MoSe_2$ and the 2.3-nm PbS QDs was studied by the same procedure. The differential reflection signal obtained with

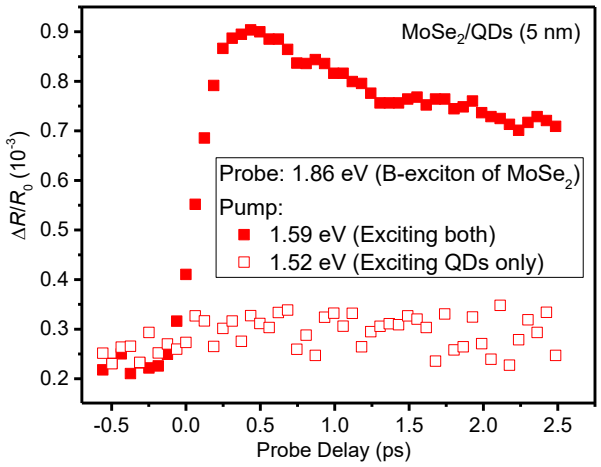

FIG. 6. Differential reflection signals from the $MoSe_2$/QDs (5 nm) heterostructure measured with a 1.86-eV probe and with pumps with different photon energies. The 1.59-eV pump (solid symbols) excites both the $MoSe_2$ and the QDs, while the 1.52-eV (open symbols) can only excite the QDs.

the 1.87-eV pump and 1.58-eV probe is shown as the blue symbols in Figure 4. The decay of the signal can be fit by a bi-exponential function, as shown by the magenta curve over the blue symbols. The two components are $\tau_1 = 0.6 \pm 0.06$ ps (45%) and $\tau_2 = 56 \pm 2$ ps (55%). In addition, there is a significant long-lived signal, although not as long as in the first heterostructure. We attribute the 56-ps process to the hole transfer from $MoSe_2$ to the 2.3-nm PbS QDs. The slower transfer rate is consistent with the smaller energy offset for holes in this heterostructure. To study a potential electron transfer process from the 2.3-nm QDs to $MoSe_2$, we used the same scheme as shown in Figure 6. Similarly, no signal was observed when we only pump 2.3-nm QDs (with the 1.52-eV pump), confirming the absence of electron transfer from 2.3-nm QDs to $MoSe_2$, similar to the 5-nm QDs.

C. Charge Transfer between MoS_2 Monolayer and PbS Quantum Dots

In this sub-section, we discuss the charge transfer properties of the heterostructures formed by MoS_2 monolayers and PbS QDs. The experimental approach is similar to the $MoSe_2$-based heterostructures discussed in the previous sub-section. The inset of Figure 7 shows the band alignment of the MoS_2QDs (5 nm) heterostructure based on the energy diagram of the 5-nm QDs shown in Figure 1(c) and previously reported values for monolayer MoS_2[36]. Similar to the $MoSe_2$-based heterostructures, here the band alignment is also type-II for both sizes of the QDs.

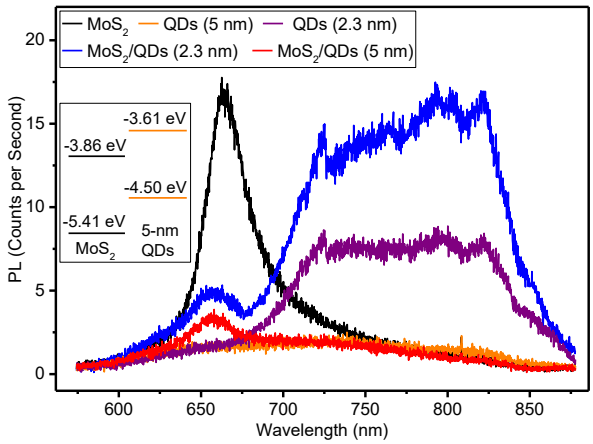

FIG. 7. Photoluminescence spectra from the monolayer MoS_2 (black), the 5-nm PbS QDs (orange), the 2.3-nm PbS QDs (purple), the MoS_2/QDs (5 nm) heterostructure (red), and the MoS_2/QDs (2.3 nm) heterostructure (blue). All the spectra were taken under the same excitation condition of 405 nm and 5 μW. The inset shows the expected band alignment of the MoS_2/QDs (5 nm) heterostructure.

First we obtained the PL spectra from different samples, as shown in Figure 7. The measurement was performed under the same conditions as the $MoSe_2$-based samples. As shown by the black curve, the monolayer MoS_2 sample shows a PL peak at 664 nm (1.87 eV), which is from the recombination of the A-excitons. The PL spectra of the 2.3-nm and 5-nm QDs (purple and orange) have been discussed in the previous sub-section. For the heterostructure formed by MoS_2 and the 2.3-nm QDs (blue), the peak associated with the QDs is increased by a factor of 2, while the MoS_2 peak is decreased by a factor of about 3. The less pronounced PL quenching of MoS_2, compared to $MoSe_2$-based heterostructures, follows the trend that in 2D-2D heterostructures MoS_2 usually shows less PL quenching due to its poor PL yield[40]. For the heterostructure formed by MoS_2 and the 5-nm QDs (red), the MoS_2 peak is quenched by a factor of 5.

Transient absorption measurements were performed to studied photocarrier dynamics in these samples. For the monolayer MoS_2 sample, a 3.18-eV pump pulse with an energy fluence of 15 μJ cm^{-2} was used to inject photocarriers and a 1.87-eV probe monitored their dynamics. The result is shown by the black symbols in Figure 8. The decay of the signal was fit by a tri-exponential function as shown by the magenta curve over the black symbols. The three time constants are τ_1 = 0.6 ± 0.02 ps (45%), τ_2 = 13 ± 2 ps (35%), and τ_3 = 25 ± 5 ps (20%). The τ_1 process is attributed to the exciton formation process, similar to the $MoSe_2$ monolayers. The long time constant of 25 ps agrees well with the previously reported exciton lifetime in CVD MoS_2 monolayers[43]. The in-

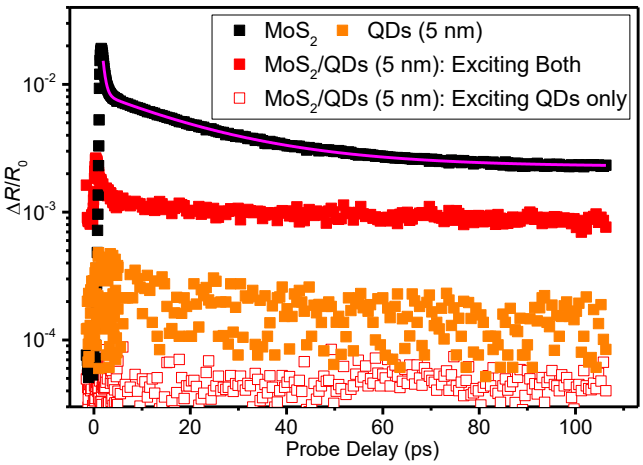

FIG. 8. Differential reflection signal of the MoS_2 monolayer (black), the 5-nm PbS QDs (orange), and the MoS_2/QDs heterostructure (red solid). In all these measurements, the pump and probe photon energies are 3.18 and 1.87 eV, respectively. The red open symbols show the result from the heterostructure when the pump photon energy is changed to 1.59 eV (and thus can excite the QDs only).

termediate time constant of 13 ps could be attributed to additional exciton recombination channels such as exciton-exciton annihilation. The differential reflection signal from the heterostructure formed by monolayer MoS_2 and the 5-nm QDs (solid red symbols) is very different from that of monolayer MoS_2. Similar to the $MoSe_2$/QD (5 nm) heterostructure, we also observed a long-lived signal with a large residual, indicating hole transfer from MoS_2 to the 5-nm QDs. The 33-ps decay time is assigned to this transfer process. To rule out the contribution from the QDs to the signal, we repeated the measurement on the 5-nm PbS QDs, no signal was detected, as shown by the orange symbols. To study a potential electron transfer process from the 5-nm QDs to MoS_2, we tuned the pump photon energy to 1.59 eV, which is below the optical bandgap of MoS_2 and thus can only excite the QDs. With the same 1.87-eV probe as before, we did not observe a signal (red open symbols). This shows that electrons do not transfer from the 5-nm QDs to MoS_2, which is also similar to the $MoSe_2$-based heterostructures.

Finally, we repeated the measurements shown in Figure 8 with the samples based on the 2.3-nm QDs. The results are summarized in Figure 9. In contrast to the previous heterostructures, the photocarrier dynamics in the MoS_2/QDs (2.3 nm) heterostructure (solid blue symbols) is similar to that of monolayer MoS_2 (black). The lack of a long-lived signal suggests that the hole transfer from MoS_2 to the 2.3-nm QDs is insignificant. Furthermore, to study a potential electron transfer

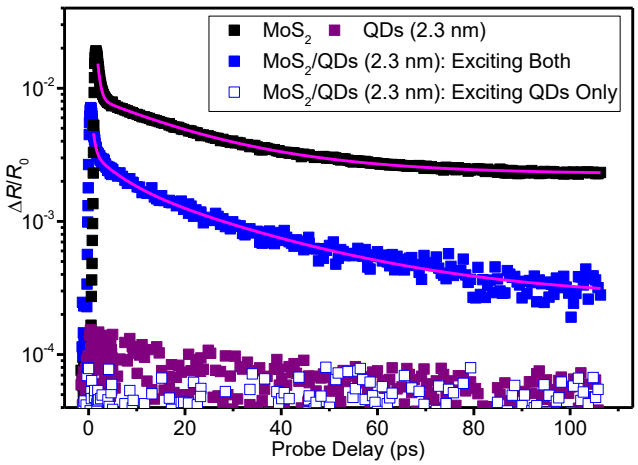

FIG. 9. Differential reflection signal of the monolayer MoS_2 (black), the 2.3-nm PbS QDs (purple), and the MoS_2/QDs heterostructure (blue solid symbols). In all these measurements, the pump and probe photon energies are 3.18 and 1.87 eV, respectively. The blue open symbols show the result from the heterostructure when the pump photon energy is changed to 1.59 eV (and thus can excite the QDs only).

from the 2.3-nm QDs to MoS_2, we used a 1.59-eV pump to excite the QDs only. As shown by the open blue symbols in Figure 9, no signal was detected (and thus no electron transfer), similar to all previously discussed heterostructures.

IV. CONCLUSION

In summary, we have studies charge transfer properties in several 0D-2D heterostructures formed by PbS QDs and TMD monolayers. Both steady-state and time-resolved optical measurements were used to study photocarrier dynamics in the heterostructures in comparison with the individual materials of QDs and TMD monolayers. For the $MoSe_2$-based heterostructures, we observed efficient hole transfer from $MoSe_2$ to PbS QDs with diameters of 5 and 2.3 nm. However, despite of their type-II band alignment, electron transfer from the QDs to $MoSe_2$ is insignificant. Similar charge transfer properties were observed in the heterostructure of monolayer MoS_2 and 5-nm PbS QDs. In contrast, no charge transfer was observed between MoS_2 and 2.3-nm QDs. These results provide useful information for understanding mechanisms of charge transfer in 0D-2D heterostructure and for developing PbS QD-based mixed-dimensional materials.

We are grateful for the financial support of National Science Foundation of USA (DMR-

1505852) and KU Research GO project.

* huizhao@ku.edu

[1] K. S. Novoselov, A. K. Geim, S. V. Morozov, D. Jiang, Y. Zhang, S. V. Dubonos, I. V. Grigorieva, and A. A. Firsov, Science **306**, 666 (2004).

[2] Z. Lin, A. McCreary, N. Briggs, S. Subramanian, K. H. Zhang, Y. F. Sun, X. F. Li, N. J. Borys, H. T. Yuan, S. K. Fullerton-Shirey, A. Chernikov, H. Zhao, S. McDonnell, A. M. Lindenberg, K. Xiao, B. J. LeRoy, M. Drndic, J. C. M. Hwang, J. Park, M. Chhowalla, R. E. Schaak, A. Javey, M. C. Hersam, J. Robinson, and M. Terrones, 2D Mater. **3**, 042001 (2016).

[3] A. K. Geim and I. V. Grigorieva, Nature **499**, 419 (2013).

[4] Y. Liu, N. O. Weiss, X. Duan, H.-C. Cheng, Y. Huang, and X. Duan, Nat. Rev. Mater. **1**, 16042 (2016).

[5] K. S. Novoselov, A. Mishchenko, A. Carvalho, and A. H. C. Neto, Science **353**, 461 (2016).

[6] B. O. Dabbousi, J. Rodriguez-Viejo, F. V. Mikulec, J. R. Heine, H. Mattoussi, R. Ober, K. F. Jensen, and M. G. Bawendi, J. Phys. Chem. B **101**, 9463 (1997).

[7] S. Kim, B. Fisher, H.-J. Eisler, and M. Bawendi, J. Am. Chem. Soc. **125**, 11466 (2003).

[8] F. Prins, A. J. Goodman, and W. A. Tisdale, Nano Lett. **14**, 6087 (2014).

[9] D. Prasai, A. R. Klots, A. K. M. Newaz, J. S. Niezgoda, N. J. Orfield, C. A. Escobar, A. Wynn, A. Efimov, G. K. Jennings, S. J. Rosenthal, and K. I. Bolotin, Nano Lett. **15**, 4374 (2015).

[10] A. Raja, A. Montoya-Castillo, J. Zultak, X. X. Zhang, Z. L. Ye, C. Roquelet, D. A. Chenet, A. M. van der Zande, P. Huang, S. Jockusch, J. Hone, D. R. Reichman, L. E. Brus, and T. F. Heinz, Nano Lett. **16**, 2328 (2016).

[11] S. Sampat, T. L. Guo, K. H. Zhang, J. A. Robinson, Y. Ghosh, K. P. Acharya, H. Htoon, J. A. Hollingsworth, Y. N. Gartstein, and A. V. Malko, ACS Photonics **3**, 708 (2016).

[12] M. X. Li, J. S. Chen, P. K. Routh, P. Zahl, C. Y. Nam, and M. Cotlet, Adv. Funct. Mater. **28**, 1707558 (2018).

[13] K. M. Goodfellow, C. Chakraborty, K. Sowers, P. Waduge, M. Wanunu, T. Krauss, K. Driscoll, and A. N. Vamivakas, Appl. Phys. Lett. **108**, 021101 (2016).

[14] H. D. Zang, P. K. Routh, Y. Huang, J. S. Chen, E. Sutter, P. Sutter, and M. Cotlet, ACS Nano **10**, 4790 (2016).

[15] H. S. Ra, D. H. Kwak, and J. S. Lee, Nanoscale **8**, 17223 (2016).

[16] C. Hu, D. D. Dong, X. K. Yang, K. K. Qiao, D. Yang, H. Deng, S. J. Yuan, J. Khan, Y. Lan, H. S. Song,

and J. Tang, Adv. Funct. Mater. **27** (2017).

[17] Y. Yu, Y. T. Zhang, X. X. Song, H. T. Zhang, M. X. Cao, Y. L. Che, H. T. Dai, J. B. Yang, H. Zhang, and J. Q. Yao, ACS Photonics **4**, 950 (2017).

[18] S. Pak, Y. Cho, J. Hong, J. Lee, S. Lee, B. Hou, G. H. An, Y. W. Lee, J. E. Jang, H. Im, S. M. Morris, J. I. Sohn, S. Cha, and J. M. Kim, ACS Appl. Mater. Interfaces **10**, 38264 (2018).

[19] A. Y. Lee, H. S. Ra, D. H. Kwak, M. H. Jeong, J. H. Park, Y. S. Kang, W. S. Chae, and J. S. Lee, ACS Appl. Mater. Interfaces **10**, 16033 (2018).

[20] R. K. Ulaganathan, K. Yadav, R. Sankar, F. C. Chou, and Y. T. Chen, Adv. Mater. Interfaces **6**, 1801336 (2019).

[21] X. Hou, H. Zhang, C. S. Liu, S. J. Ding, W. Z. Bao, D. W. Zhang, and P. Zhou, Small **14**, 1800319 (2018).

[22] L. Hu, J. Yuan, Y. Ren, Y. Wang, J. Q. Yang, Y. Zhou, Y. J. Zeng, S. T. Han, and S. C. Ruan, Adv. Mater. **30**, 1801232 (2018).

[23] A. Boulesbaa, K. Wang, M. Mahjouri-Samani, M. Tian, A. A. Puretzky, I. Ivanov, C. M. Rouleau, K. Xiao, B. G. Sumpter, and D. B. Geohegan, J. Am. Chem. Soc. **138**, 14713 (2016).

[24] S. A. McDonald, G. Konstantatos, S. Zhang, P. W. Cyr, E. J. Klem, L. Levina, and E. H. Sargent, Nat. Mater. **4**, 138 (2005).

[25] I. Moreels, K. Lambert, D. Smeets, D. De Muynck, T. Nollet, J. C. Martins, F. Vanhaecke, A. Vantomme, C. Delerue, G. Allan, *et al.*, ACS Nano **3**, 3023 (2009).

[26] C.-H. M. Chuang, P. R. Brown, V. Bulović, and M. G. Bawendi, Nat. Mater. **13**, 796 (2014).

[27] L. Bakueva, S. Musikhin, M. Hines, T.-W. Chang, M. Tzolov, G. D. Scholes, and E. Sargent, Appl. Phys. Lett. **82**, 2895 (2003).

[28] D. A. Chenet, O. B. Aslan, P. Y. Huang, C. Fan, A. M. van der Zande, T. F. Heinz, and J. C. Hone, Nano Lett. **15**, 5667 (2015).

[29] Q. Cui, R. A. Muniz, J. Sipe, and H. Zhao, Phys. Rev. B. **95**, 165406 (2017).

[30] P. Zereshki, Y. Wei, F. Ceballos, M. Z. Bellus, S. D. Lane, S. Pan, R. Long, and H. Zhao, Nanoscale **10**, 11307 (2018).

[31] M. M. Tavakoli, A. Simchi, Z. Fan, and H. Aashuri, Chem. Comm. **52**, 323 (2016).

[32] M. M. Tavakoli, H. Aashuri, A. Simchi, and Z. Fan, Phys. Chem. Chem. Phys. **17**, 24412 (2015).

[33] M. Tavakoli, A. Simchi, and H. Aashuri, Mater. Chem. Phys. **156**, 163 (2015).

[34] A. Tayyebi, M. M. Tavakoli, M. Outokesh, A. Shafiekhani, and A. Simchi, Ind. Eng. Chem. Res **54**,

7382 (2015).

[35] F. Ceballos and H. Zhao, Adv. Funct. Mater. **27**, 1604509 (2017).

[36] Y. Guo and J. Robertson, Appl. Phys. Lett. **108**, 233104 (2016).

[37] H. Fang, C. Battaglia, C. Carraro, S. Nemsak, B. Ozdol, J. S. Kang, H. A. Bechtel, S. B. Desai, F. Kronast, A. A. Unal, *et al.*, Proc. Natl. Acad. Sci. U.S.A **111**, 6198 (2014).

[38] M. M. Furchi, A. Pospischil, F. Libisch, J. Burgdörfer, and T. Mueller, Nano Lett. **14**, 4785 (2014).

[39] S. Q. Zhao, D. W. He, J. Q. He, X. W. Zhang, L. X. Yi, Y. S. Wang, and H. Zhao, Nanoscale **10**, 9538 (2018).

[40] F. Ceballos, P. Zereshki, and H. Zhao, Phys. Rev. Mater. **1**, 044001 (2017).

[41] T. R. Kafle, B. Kattel, P. Yao, P. Zereshki, H. Zhao, and W. L. Chan, J. Am. Chem. Soc. **141**, 11328 (2019).

[42] M. Z. Bellus, Z. Yang, P. Zereshki, J. Hao, S. P. Lau, and H. Zhao, Nanoscale Horiz. **4**, 236 (2018).

[43] X. F. Liu, H. Y. Yu, Q. Q. Ji, Z. H. Gao, S. F. Ge, J. Qiu, Z. F. Liu, Y. F. Zhang, and D. Sun, 2D Mater. **3**, 014001 (2016).